Temperature-Responsive Fibers of Cellulose-Based Copolymers

Ana C. Santos[1, 2], Sérgio Alves[1], Maria H. Godinho[2], Carlos Baleizão[1*], José Paulo S. Farinha[1*]

[1] Centro de Estrutural and IN−Institute of Nanoscience and Nanotechnology, Instituto Superior Técnico, 1049-001 Lisboa, Portugal

[2] I3N-CENIMAT and Department of Materials Science, New University of Lisbon, 2829-516 Caparica, Portugal

* Corresponding authors, email: carlos.baleizao@tecnico.ulisboa.pt; farinha@tecnico.ulisboa.pt

Supplementary Information

Contents

Synthesis of Acetyl Propargyl Cellulose (CAPr)

The efficiency of CA modification with propargyl groups was evaluated by ^{1}H NMR. Around 3.44 ppm we observe 3 signals assigned to the propargyl CH_2 group (Figure S1). These signals are slightly shifted depending on the position where the substitution occurs.

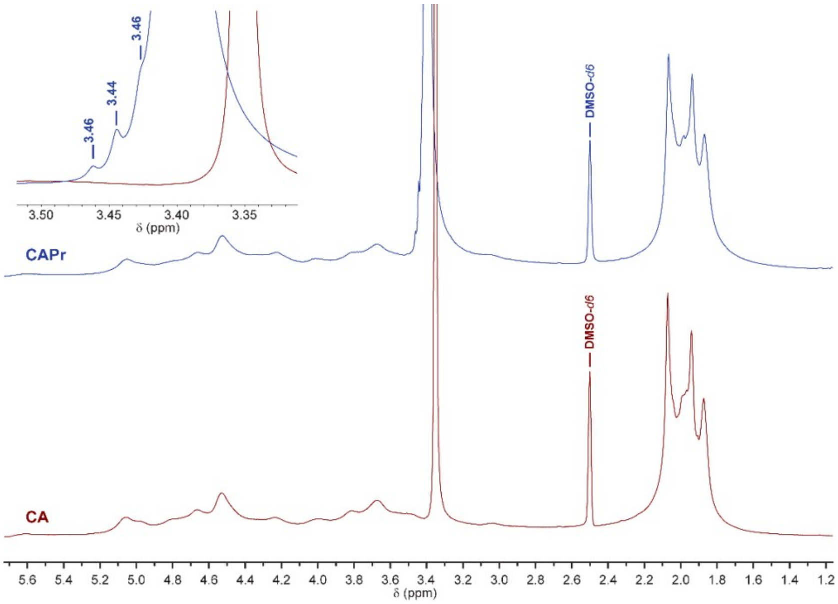

Figure S1 – ^{1}H NMR spectra of CA and CAPr. Both spectra are similar in terms of signals and integration. The only slight difference is found near 3.44 ppm. The signals are assigned to the propargyl CH_2 group.

Since the signals fall in the same region of the water peak, we perform a signal deconvolution that allowed us to verify that about 4% of the integral of this region corresponds to propargyl CH_2 groups (Figure S2).

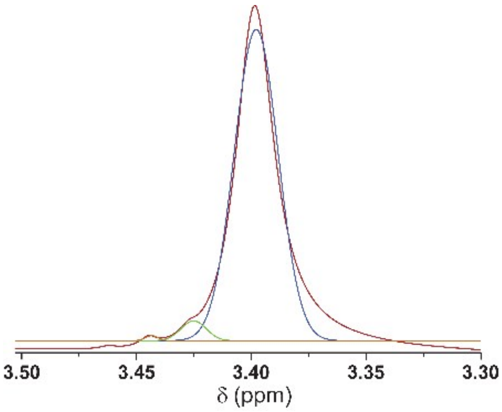

Figure S2 – Deconvolution of 1H NMR signals of water (3.40 ppm) and propargyl CH_2 (3.46 -3.42 ppm).

The ratio between the protons of acetate groups (2.30 – 1.7 ppm) and the protons of propargyl groups (2.46-2.42 ppm) yield 0.35 propargyl groups per monomer of CA. According to the CA supplier there is one remaining OH group per monomer of CA, so that the substitution of the acetate groups by propargyl was achieved with 35% yield.

Synthesis of AHMA

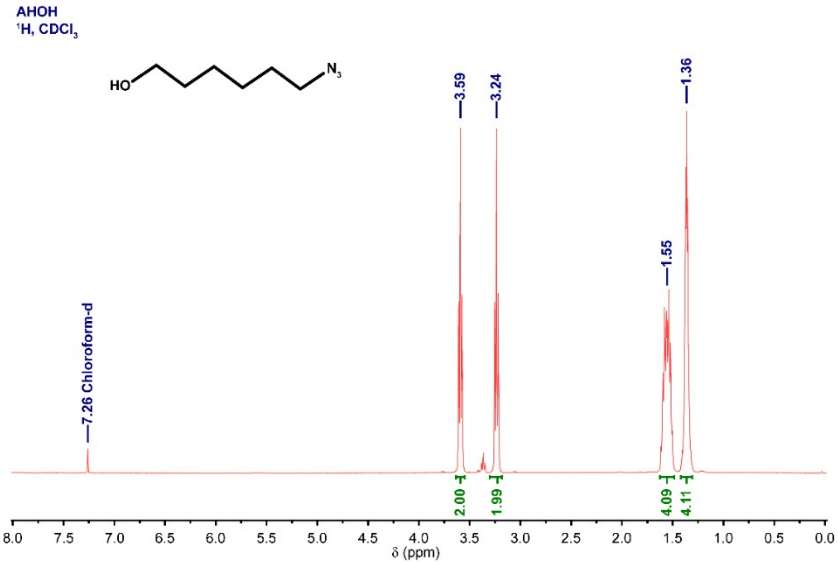

Figure S3 - NMR spectrum of AHOH. ^{1}H NMR (400 MHz, ($CDCl_3$): δ (ppm) 1.36 - 1.55 (8H, m, CH_2-CH_2-CH_2-CH_2), 3.24 (2H, t, N_3-CH_2), 3.59 (2H, t, O-CH_2).

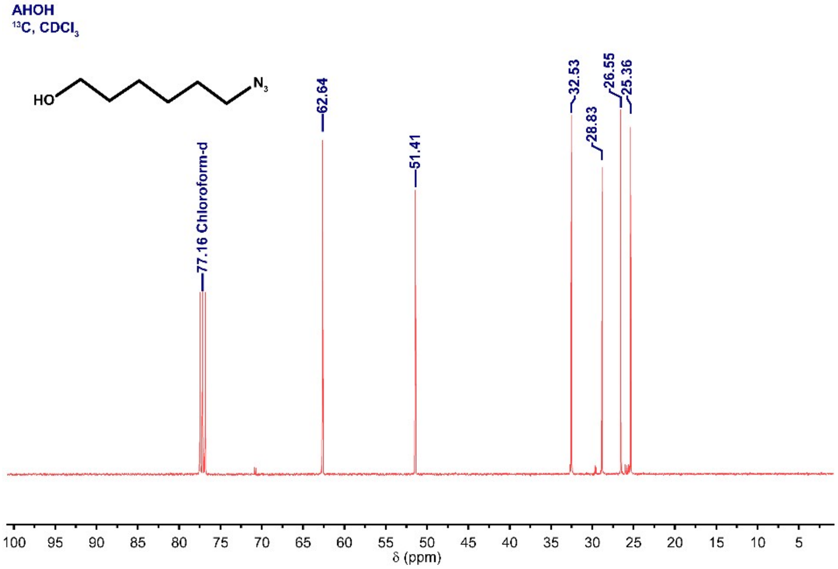

Figure S4 - NMR spectrum of AHOH. ^{13}C NMR (500 MHz, $CDCl_3$): 25.36, 26.55, 28.83, 51.41, 62.64.

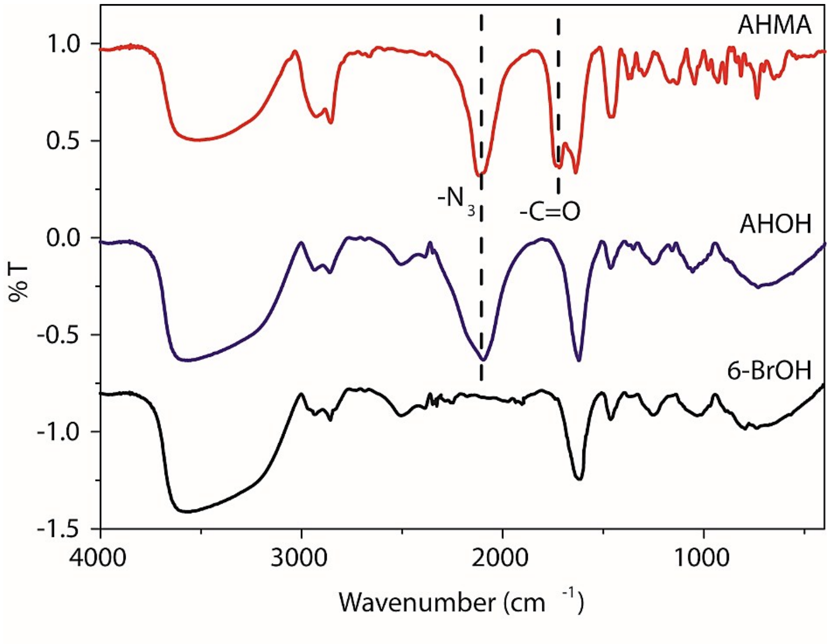

Figure S5 – FTIR spectrum of AHOH and AHMA in NaCl disks.

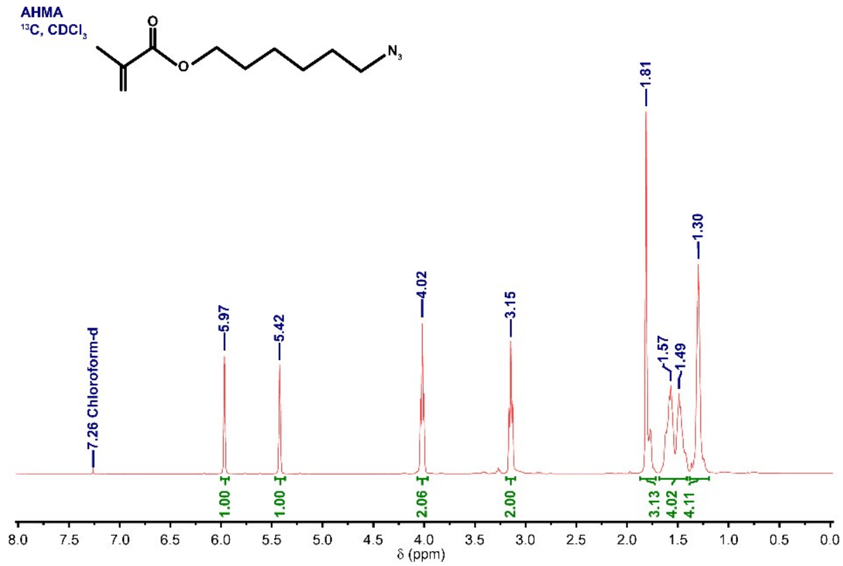

Figure S6 - NMR spectrum of AHMA.^1H NMR (400MHz, $CDCl_3$): δ (ppm) 1.30 (m, 4H, CH_2), 1.49 - 1.59 (m, 4H, CH_2), 1. 81 (s, 3H, CH_3), 3.15 (t, 2H, CH_2N_3), 4.02 (t, 2H, CH_2O), 5.42 (s, 1H, =CH), 5.97 (s, 1H, =CH).

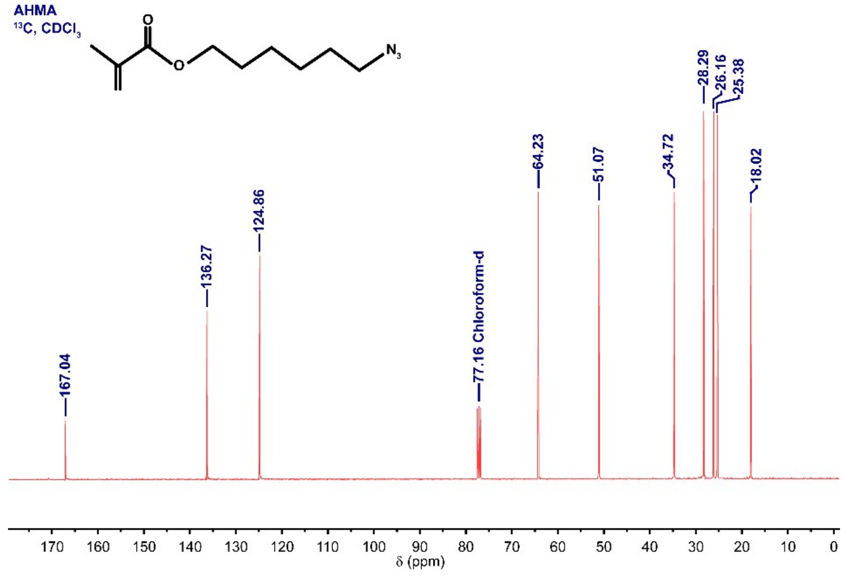

Figure S7 - NMR spectrum of AHMA. ^{13}C NMR (500 MHz, $CDCl_3$): 18.02, 25.38, 26.16, 28.29, 34.72, 51.07, 64.23, 124.86, 136.27, 167.04.

Synthesis of p(MEO_2MA-co-OEGMA-b-AHMA)

Before the beginning of polymerization reaction, the relative proportion of the two first monomers in the monomer feed was confirmed by NMR. The NMR spectra of MEO_2MA and OEGMA presents no differences in terms of chemical shifts. The only difference is the area of signals between 3.5 and 4.25 ppm, which were assigned to PEG protons. MEO_2MA presents a signal corresponding to 8 protons in the mentioned zone. OEGMA presents 36 protons in the same area, Figure S8. As we prepared the polymerization reaction we took a sample of the two monomers mixed and evaluate by NMR the proportion based on the integration of these signals, Figure S9. The proportion between the two monomers is given by Eq. 1.

$$\int \delta(4.3 - 3.5ppm) = f(M_1).{}^1H(M_1) + \left[1 - f(M_1)\right].{}^1H(M_2) \qquad \text{Eq (1)}$$

Where $\int \delta(4.3 - 3.5ppm)$ is the area of the signals in the PEG protons region, $f(M_1)$ is the relative proportion of MEO_2MA, ${}^1H(M_1)$ is the number of PEG protons on MEO_2MA, which is 8, and ${}^1H(M_2)$ is the number of PEG protons on OEGMA, which is 36. Using this equation, we establish the proportion of 93% of MEO_2MA and 7% of OEGMA.

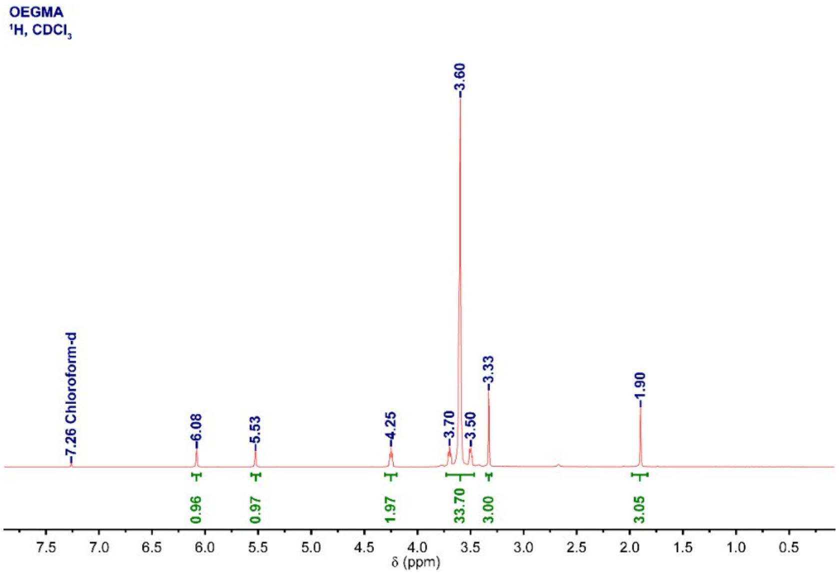

Figure S8 - NMR spectrum of OEGMA. ^1H NMR (400MHz, $CDCl_3$): δ (ppm) 1.90 (s, 3H, C-CH_3), 3.33 (s, 3H, O-CH_3), 3.50-4.25 (m, 36H, -O-CH_2-CH_2-), 5.53 (s, 1H, =CH_2), 6.08 (s, 1H, =CH_2).

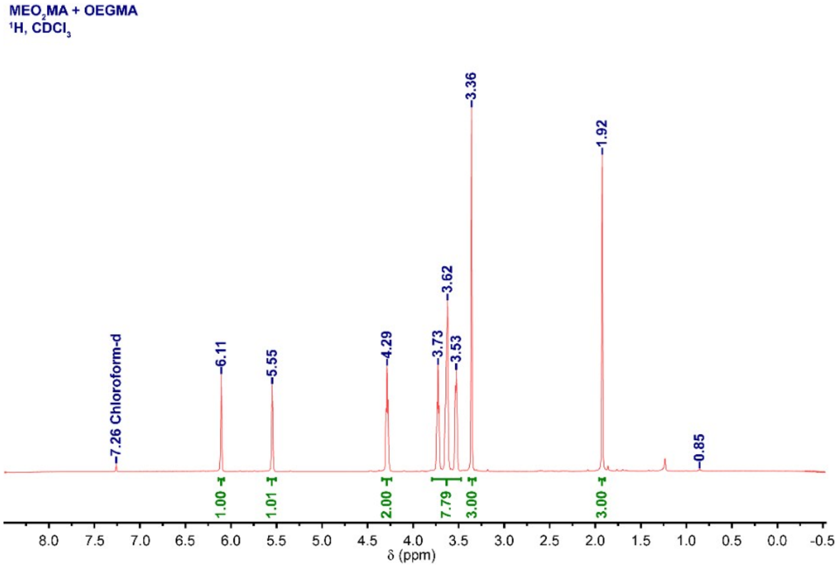

Figure S9 - NMR spectrum of MEO_2MA and OEGMA comonomer feed at t=0. ^1H NMR (400MHz, $CDCl_3$): δ (ppm) 1.90 (s, 3H, C-CH_3), 3.33 (s, 3H, O-CH_3), 3.50-4.25 (m, 10H, -O-CH_2-CH_2-), 5.53 (s, 1H, =CH_2), 6.08 (s, 1H, =CH_2).

The polymerization was followed by NMR. Samples were periodically withdrawn from the polymerization medium for analysis. To follow the kinetics, individual monomer conversions were determined by ^1H NMR (Figure S10). As internal reference we used the signal assigned to the terminal methyl protons at the end of the PEG chains once this signal keeps constant during the reaction. The relation between the signals of terminal methyl protons and the vinylic protons was used to evaluate the conversion. The global conversion is calculated from the individual monomer conversions, Eq 2.

$$Global\ conversion = 1 - \frac{M}{M_0} = \frac{[M_1]_0 . conversion\ of M_1 + [M_2]_0 . conversion\ of M_2}{[M_1]_0 + [M_2]_0} \qquad \text{Eq (2)}$$

As the individual signals of each monomer are indistinguishable, we considered that the reactivities of both monomers are comparable, so the Eq. 2 is simplified to:

$$Global\ conversion = 1 - \frac{M}{M_0} = \frac{[M]_0 . conversion\ of M}{[M_1]_0 + [M_2]_0} \qquad \text{Eq. (3)}$$

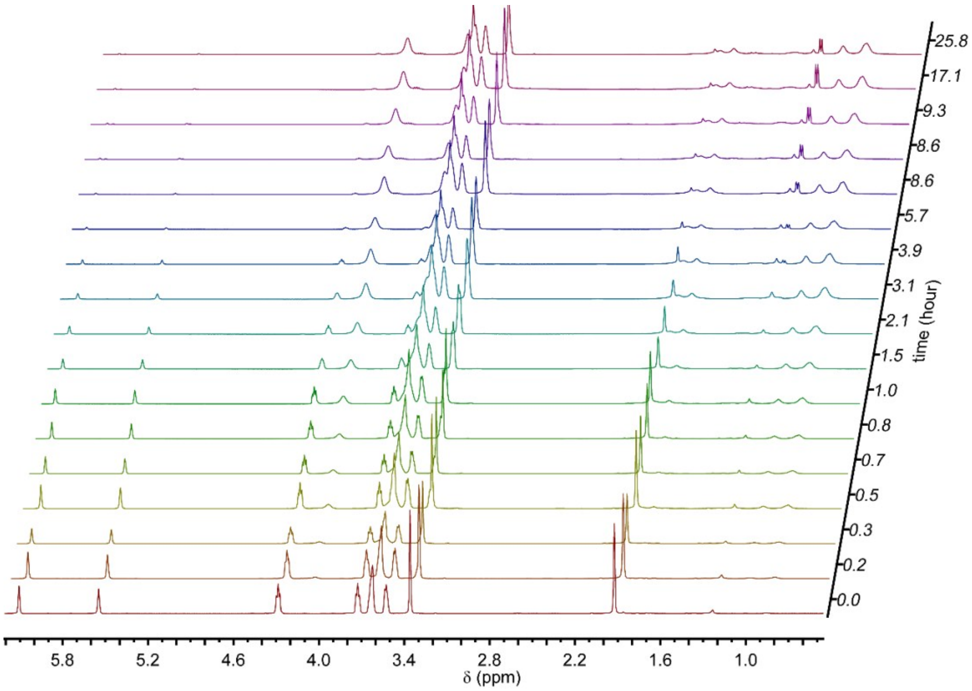

Figure S10 - ^{1}H NMR spectra of polymerization reaction samples with time in $CDCl_3$. It is evident the disappearance of 5.53 and 6.08 ppm signals with time, which are assigned to $=CH_2$ protons in the monomer structure. Moreover, it is possible to notice two significant shifts: the methyl group of the methacrylate at 1.90 ppm is shifted to lower values at the polymer structure and the first -CH2- of the PEG chains shifts from 4.30 to 4.0 ppm.

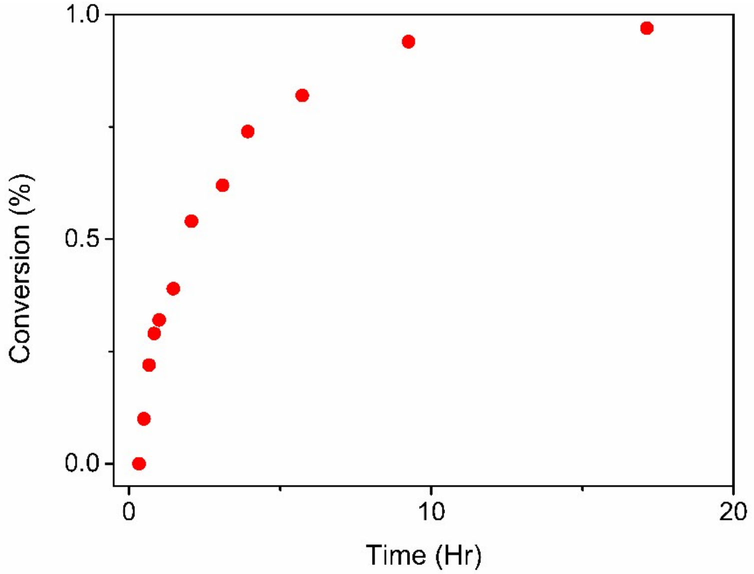

Figure S11 – Time evolution of monomer conversion for copolymerization of MEO_2MA with OEGMA in isopropyl alcohol at 90°C, using AIBN as initiator. ($[M]_0/[CTA]=83$, $[M]_0=0.1 mol.L^{-1}$ and $[CTA]/[AIBN]=10$).

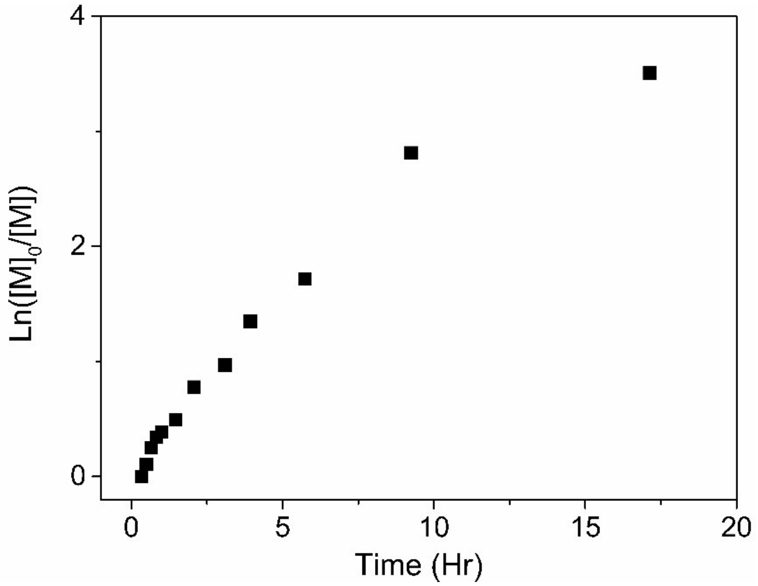

Figure S12 - Kinetic plot for RAFT copolymerization of MEO$_2$MA with OEGMA in isopropyl alcohol at 90°C using AIBN as initiator. ($[M]_0/[CTA]=83$, $[M]_0=0.1 mol.L^{-1}$ and $[CTA]/[AIBN]=10$).

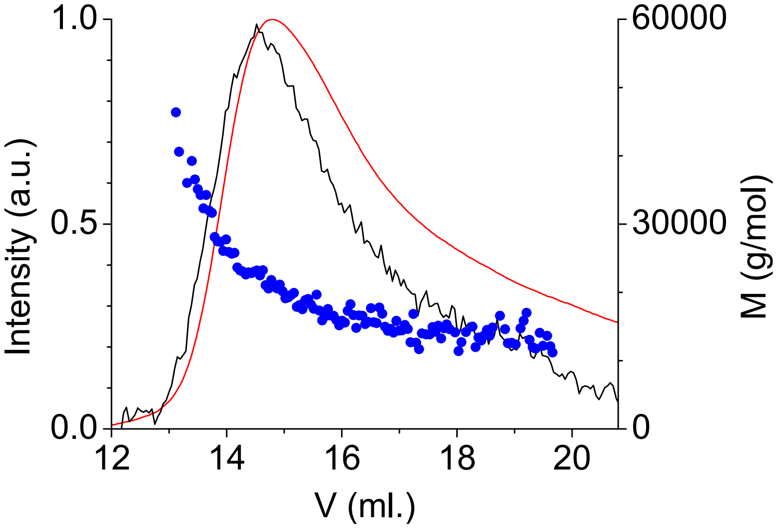

Figure S13 – GPC/SEC chromatogram of the TRP. Refractive index (RI) signal (red) and multiangle light scattering (MALS) signal at 90° (black) vs elution volume. Molecular weight calculated for each elution volume (blue dots)

Surface studies of spin-coated films

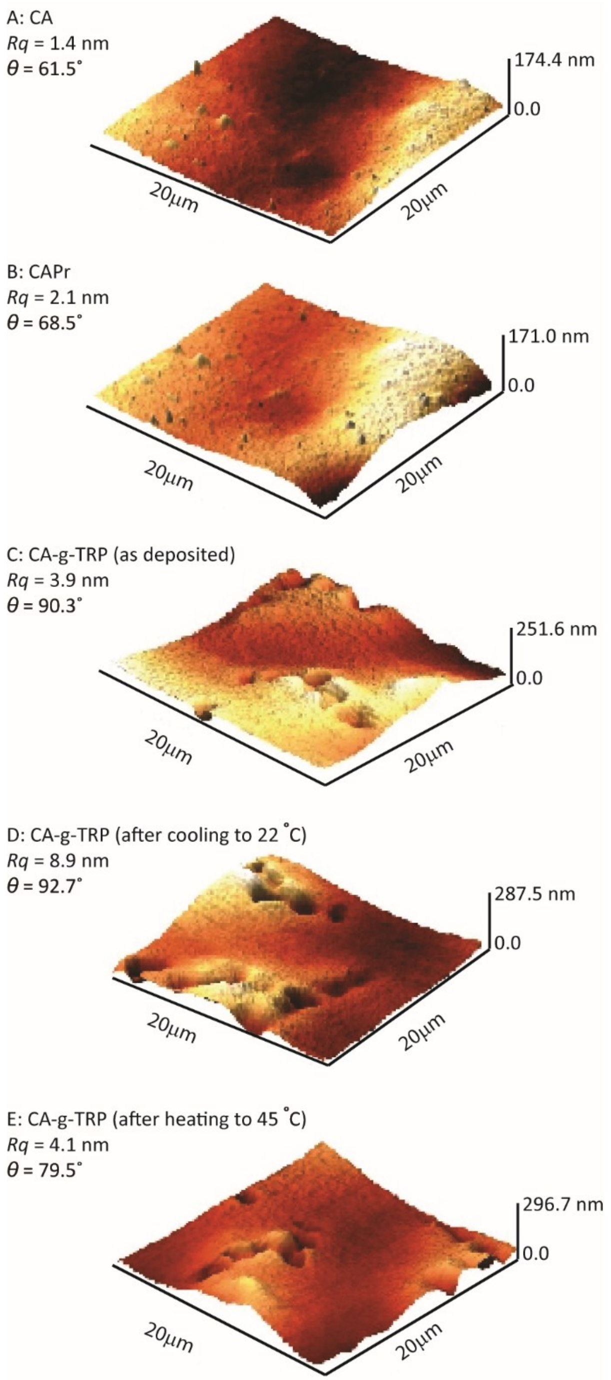

Figure S14 - Root mean square roughness R_q obtained from amplitude AFM images and contact angle measurements of film surfaces: CA (A), CAPr (B) and CA-g-TRP as deposited (C), after cold water treatment at 22 ˚ C (D) and after hot water treatment at 45 ˚ C (E). Contact angle values obtained for the same films are also indicated. All films were deposited by spin coating from 20wt% solutions of each compound in DMAC/Acetone (2:1). Contact angle between the surface and a water droplet measured by the sessile drop method.

Temperature response of p(MEO$_2$MA-*co*-OEGMA-*b*-AHMA)

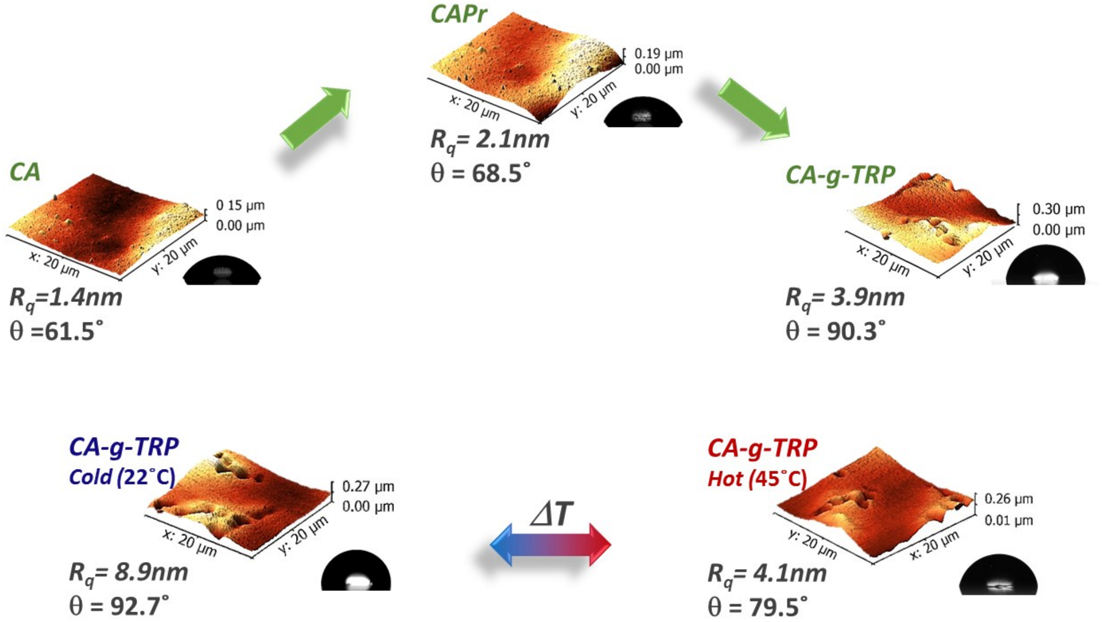

Figure S15 – Morphological characterization and contact angle measurements of film surfaces: CA , CAPr and CA-g-TRP as deposited , after cold water treatment and after hot water treatment. Both films were deposited by blade casting from 20 wt% solutions in DMAC/Acetone (2:1).